Structural basis for the interaction of Redβ single strand annealing protein with *Escherichia coli* single-stranded DNA binding protein.

Katerina Zakharova[1,§], Mengqi Liu[1,§], Jacelyn R. Greenwald[3,§], Dr. Brian C. Caldwell[1,2], Zihao Qi[3], Dr. Vicki H. Wysocki[2,3], and Dr. Charles E. Bell[1,2,3,*]

[1] *Department of Biological Chemistry and Pharmacology, The Ohio State University, Columbus, OH, USA*

[2] *Ohio State Biochemistry Program, The Ohio State University, Columbus, OH, USA*

[3] *Department of Chemistry and Biochemistry, The Ohio State University, Columbus, OH, USA*

***Correspondence to:** Charles E. Bell: **bell.489@osu.edu**; 614-323-3225; 1060 Carmack Road, 226B Rightmire Hall, Columbus OH 43210.*

§ These authors contributed equally to this work.

Keywords: Recombineering, SSB, DNA Repair, Native Mass Spectrometry, DNA Replication

Abstract

Redβ is a protein from bacteriophage λ that binds to single-stranded DNA (ssDNA) to promote the annealing of complementary strands. Together with λ exonuclease (λ-exo), Redβ is part of a two-component DNA recombination system involved in multiple aspects of genome maintenance. The proteins have been exploited in powerful methods for bacterial genome engineering in which Redβ can anneal an electroporated oligonucleotide to a complementary target site at the lagging strand of a replication fork. Successful annealing *in vivo* requires the interaction of Redβ with *E. coli* single-stranded DNA binding protein (SSB), which coats the ssDNA at the lagging strand to coordinate access of numerous replication proteins. Previous mutational analysis revealed that the interaction between Redβ and SSB involves the C-terminal domain (CTD) of Redβ and the C-terminal tail of SSB (SSB-Ct), the site for binding of numerous host proteins. Here, we have determined the x-ray crystal structure of Redβ CTD in complex with a peptide corresponding to the last nine residues of SSB (MDFDDDIPF). Formation of the complex is predominantly mediated by hydrophobic interactions between two phenylalanine side chains of SSB (Phe-171 and Phe-177) and an apolar groove on the CTD, combined with electrostatic interactions between the C-terminal carboxylate of SSB and Lys-214 of the CTD. Mutation of any of these residues to alanine significantly disrupts the interaction of full-length Redβ and SSB proteins. Structural knowledge of this interaction will help to expand the utility of Redβ-mediated recombination to a wider range of bacterial hosts for applications in synthetic biology.

Introduction

Redβ is a 261-amino acid (M_r 29.6 kDa) protein from bacteriophage λ that binds to single-stranded DNA (ssDNA) to promote the annealing of complementary strands (1,2). It functions together with an exonuclease (λ-exo) as part of a two-component DNA recombination system with potential roles in replication, genome packaging, repair of dsDNA breaks, and promotion of genetic diversity (3,4). A schematic overview of the system is shown in Figure 1. First, λ-exo binds to double-stranded DNA (dsDNA) ends and resects the 5'-strand to form a long 3'-overhang (5-7). Redβ then assembles on the 3'-overhang to promote its annealing with a complementary DNA strand. The two proteins form a complex that is thought to mediate loading of Redβ directly onto the 3'-overhang as it is generated by λ-exo (8,9). Binding of Redβ to λ-exo is mediated by its C-terminal domain (CTD, residues 194-261), whereas its N-terminal domain (NTD, residues 1-177) is responsible for DNA binding and oligomerization (10,11).

Homologs of λ-exo and Redβ are encoded in the genomes of a wide variety of bacteriophage with dsDNA genomes (12). While their precise roles for phage propagation have been elusive, the proteins have been exploited in powerful methods for bacterial genome engineering known as recombineering and multiplexed automated genome engineering (MAGE) (13-15). In one type of recombineering called single-strand oligonucleotide repair (ssOR), a synthetic oligonucleotide that is complementary to a target site but encodes an alteration is electroporated into *E. coli* cells expressing Redβ. Redβ then binds the oligonucleotide and anneals it to a target site exposed as ssDNA at the lagging strand of a replication fork (16,17). Redβ forms a protein-protein interaction with *E. coli* SSB protein (18), which coats the ssDNA at the lagging strand to protect it from degradation and coordinate access of numerous proteins involved in replication (19-21) (Figure 1C). Mutational analysis indicates that this interaction involves the acidic C-terminal tail of SSB (C-tail) and a site on Redβ CTD that overlaps with its λ-exo binding site (18). Mutations that disrupt the Redβ-SSB interaction completely abolish oligonucleotide recombination *in vivo* (18). This suggests that for a Redβ–ssDNA complex to gain access to the complementary target site on the lagging strand, it must interact with the SSB C-tail to either displace SSB and expose the ssDNA at the target site or co-localize to the lagging strand and compete with SSB for the target site.

Here, we have determined the x-ray crystal structure of the Redβ CTD in complex with a peptide corresponding to the last nine residues of SSB (SSB-Ct, residues 169-177, MDFDDDIPF). All nine residues

of the SSB peptide are ordered in the complex and bind to the expected hydrophobic groove on the surface of the CTD, largely through the insertion of two phenylalanine side chains of SSB (Phe-171 and Phe-177), as well as electrostatic interactions with the SSB C-terminal carboxylate. Mutation of residues forming key interactions in the structure to alanine significantly disrupts the complex formed by the full-length proteins, suggesting that the interactions seen in the crystal structure are functionally relevant. A dimeric form of the CTD–SSB-Ct complex was observed in all four crystal forms, but native mass spectrometry (nMS) did not detect the presence of the dimeric complex in solution. nMS also revealed that the complex between the CTD and the SSB-Ct peptide is weak, suggesting that further interactions or oligomeric assemblies may be relevant *in vivo*. Structural knowledge of the complex helps to explain prior data on the ability of Redβ and orthologous proteins to operate in bacterial hosts with different C-terminal sequences of their SSB proteins (22).

Results

Crystal Structure of Redβ CTD in complex with SSB-Ct peptide

For structural analysis, attempts to crystallize full-length Redβ with the SSB-Ct peptide did not yield crystals, likely due to flexibility between the Redβ N- and C-terminal domains and/or the non-uniform oligomerization of Redβ that has been detected by nMS (23). Since mutational data suggests that the interaction involves the CTD of Redβ and the C-tail of SSB (18), we focused on just the CTD–SSB-Ct complex for crystallization, as indicated by the magenta circle in Figure 1C, and found numerous conditions that gave large single crystals. All these conditions required the presence of the peptide for growth and contained high concentrations of salt as the main precipitant, suggesting that the complex may be stabilized to a significant degree by hydrophobic interactions. Diffraction data from four different crystal forms was collected at Beamline 31-ID of the Advanced Photon Source and refined to resolutions ranging from 1.5-1.8Å resolution (Table 1).

The four crystal forms reveal essentially the same structure, with all nine residues of the SSB-Ct peptide visible in the electron density and bound to the expected groove on the surface of the CTD (Figure 2). The N-terminal tryptophan of the peptide, which was added for concentration measurement, was also ordered in the complex but formed few interactions. As the resolution and refinement statistics are best for

Form 1, it will be described here. The CTD–SSB-Ct peptide interaction buries 1078 Å^2 of solvent-accessible surface area. The peptide is bound in a conformation with some degree of internally folded structure, with the side chains of Met-169 and Ile-175 in contact with one another and residues 170-174 bulging out to form a U-shape (Figure 2A). This conformation is partially stabilized by intra-peptide hydrogen bonds between the backbone carbonyl of Asp-170 and the backbone amide of Asp-173, the side chain carboxylate of Asp-170 and the backbone amides of Asp-172 and Asp-173, and the side chain carboxylate of Asp-173 and the backbone amide of Asp-170 (see dashed purple lines in Figure 2A).

The most prominent interactions of the complex are the insertions of the phenyl rings of Phe-171 and Phe-177 of SSB-Ct into a hydrophobic groove on the CTD that is formed by all three of its α-helices (Figure 2). The phenyl ring of Phe-177 of SSB-Ct inserts into a pocket formed by the side chains of several apolar residues of the CTD including Leu-209, Leu-212, Leu-220, Leu-223, Phe-249, Leu-250, and the aliphatic portions of Lys-214 and Asp-219. The phenyl ring of Phe-171 of SSB-Ct inserts into an adjacent pocket on the CTD formed by the side chains of Leu-220, Leu-223, Cys-224, Ile-227, Phe-228, Phe-249, and Ala-246. Leu-220, Leu-223 and Phe-249 of the CTD are part of both pockets and bridge the two (Figure 2A and B). The side chain of Ile-175 of SSB-Ct is not buried as deeply as Phe-171 and Phe-177 but does form hydrophobic interactions with Leu-223, Ile-227, and Phe-249 of the CTD.

The complex is also stabilized by electrostatic interactions. Most prominent is an ion pair between the C-terminal carboxylate of Phe-177 of SSB-Ct and the terminal amine of Lys-214 of the CTD. Lys-253 of the CTD is also close to the C-terminus of the SSB-Ct peptide as predicted (18) but contacts the backbone carbonyl of Ile-175 of SSB-Ct instead of the C-terminal carboxylate. Lys-253 also forms a distant (3.7Å) ion pair with the carboxylate of Asp-174 of SSB-Ct, although the two side chains are solvent-exposed and flexible based on their relatively high temperature factors. The side chains of the remaining residues of SSB-Ct, including Met-169, Asp-170, Asp-172, Asp-173, and Pro-176 generally point away from the CTD and do not form close interactions with it. The carboxylates of Asp-170 and Asp-172 do, however, form potential long-range electrostatic interactions (8-11Å) with a positively charged surface of the CTD formed in large part by Arg-229 and Lys-245 (Figure 2B).

As expected, SSB-Ct binds to a site on the CTD that overlaps significantly with the site for binding to λ-exo (Figure 3). Accommodation of the two different ligands is accompanied by minor changes to side chains of residues lining the apolar cleft on the CTD, which reorient in the complex with SSB-Ct to

accommodate the different binding partner. The two largest side chain movements occur in Phe-249 and Lys-253 of the CTD (Figure 3B). Reorientation of the Phe-249 side chain opens a new pocket on the CTD that allows for insertion of the phenyl ring of Phe-171 of SSB-Ct. This pocket is not occupied by λ-exo in its complex with the CTD. Similarly, Lys-253 of the CTD reorients to allow the C-terminal carboxylate of SSB-Ct to move in and contact Lys-214 of the CTD, and Lys-253 to contact Asp-174 and the backbone carbonyl of Ile-175 of SSB-Ct. Overall, SSB-Ct and λ-exo contact partially, but not completely, overlapping surfaces on the CTD, and the contours of the CTD surface change in the two structures due to side chain movements that accommodate the different binding partners.

Structure of a Redβ CTD–SSB-Ct dimer

All four crystal forms contain the same C2-symmetric dimer of the CTD–SSB-Ct complex (Figure 4), either in the asymmetric unit (Forms 1,2,4), or along a crystallographic 2-fold (Form 3). The dimer buries 1,027 $Å^2$ of total solvent accessible surface area, 223 $Å^2$ between the two protein chains, 394 $Å^2$ between the two peptides, and 631 $Å^2$ by cross protein-peptide interactions. Thus, the dimer is largely held together by interactions involving the two SSB-Ct peptides. Specifically, the side chains of Met-169, Ile-175, and Pro-176 of the two peptides come together to form hydrophobic interactions about the 2-fold axis (Figure 4B). Limited interactions involving the two CTDs are also formed. Most prominently, Gln-226 of the CTD forms a bi-dentate pair of hydrogen bonds with the backbone amide and carbonyl of Met-169 of the peptide from the neighboring complex (Figure 4C). Each Gln-226 side chain also forms a hydrogen bond with the backbone carbonyl of Gln-226 of the other subunit of the dimer. These interactions form a network of hydrogen bonds that is repeated about the 2-fold axis of symmetry. The N-terminal tryptophan of the SSB-Ct peptide forms some van der Waals interactions at the dimer interface, particularly with the side chain of Pro-222 on the CTD. The tryptophan was added to the peptide as a handle to measure its concentration and thus the interactions it forms would not be relevant to the native CTD–SSB complex.

To determine if the dimer of the CTD–SSB-Ct complex exists in solution, nMS was performed on the CTD alone and in complex with SSB-Ct peptide. For these experiments, the peptide did not contain the extra N-terminal Trp residue that was used for crystallization, as it would not be present in the physiologically relevant complex. Moreover, both 9-mer and 15-mer versions of the SSB-Ct were tested, to determine if extending further back into the SSB sequence affects complex formation. The 9-mer peptide

grew crystals with the CTD to result in essentially the same structure described above, indicating that the extra Trp residue did not affect the structure. It is therefore reasonable to directly compare the nMS data to the crystal structures. The 15-mer peptide on the other hand did not form crystals with the CTD, suggesting that some or all the additional six residues may be disordered in the complex.

nMS of the CTD alone in 200 mM ammonium acetate revealed that it is fully monomeric at 1 μM and 5 μM, but forms a small amount of dimer at 10 μM, around 10% of total species detected (Figure 5). This small amount of dimer could conceivably be due to non-specific binding in nano-electrospray ionization (nanoESI), as opposed to specific dimer formation in solution. The experimental masses of the CTD monomer and dimer matched (within 1 amu.) those calculated from the amino acid sequence of the CTD, indicating that the purified protein is fully intact and unmodified.

nMS of the CTD–SSB-Ct complex was first performed under conditions like those used for crystallization. Specifically, the CTD and SSB-Ct were mixed at concentrations of 1.06 and 1.7 mM, respectively (a molar ratio of 1 to 1.6), and then diluted to 10 μM and 16 μM in 800 mM ammonium acetate to mimic the high salt conditions of the crystals. Surprisingly, only a very small amount of the CTD–SSB-Ct complex was detected, and nearly all the CTD protein was present as a monomer that was unbound to peptide (Figure 6A). The small amount of CTD–SSB-Ct complex detected, ~1% of the total CTD, was present as a monomer, and no dimeric complex was detected. Analysis of the complex of the CTD with the 15-mer SSB-Ct peptide at double the concentration (20 μM CTD and 32 μM 15-mer peptide) yielded similar results, with ~6% of the CTD complexed with SSB-Ct peptide as a monomer, and no observation of dimer (Figure 6B). Lastly, the concentration of ammonium acetate was lowered to 200 mM to better mimic physiological ionic strength and tested with 1.5 μM CTD and a 10-fold excess of 9-mer SSB-Ct (15 μM). Again, only a very small amount of CTD–SSB-Ct complex was observed (~3% of the total CTD), which was fully monomeric (Figure 6C).

In summary, nMS indicates that the CTD exists predominantly as a monomer at concentrations ranging from 1 - 20 μM, both alone and when mixed with the SSB-Ct peptide (9-mer and 15-mer). The dimeric version of the CTD–SSB-Ct complex present in the crystal structures was not observed. nMS further indicates that the SSB-Ct peptide binds to the CTD with an affinity significantly weaker than 20 μM. This result is consistent with previous data from fluorescence anisotropy titrations indicating that while full-length Redβ binds to fluorescein-labeled SSB-Ct peptide with an apparent K_d of 11 μM, the CTD resulted in

only a slight increase in anisotropy that could not be fit to a binding curve (18). For the CTD, the lack of anisotropy increase could be due to its smaller size (10 kDa) and lack of oligomerization, as the anisotropy increase is strongly dependent on change in mass. By contrast, full-length Redβ (32 kDa) can form oligomers as large as 12-mers to produce much larger complexes (23). However, preliminary nMS experiments with full-length Redβ and SSB-Ct also indicate an unexpectedly weak interaction (data not shown).

Mutational analysis of the Redβ–SSB-Ct interaction

To evaluate the functional significance of the complex seen in the crystal structures, residues of the CTD and SSB-Ct that make key interactions in the structure were mutated to alanine in the respective full-length proteins and tested for complex formation using a Ni-spin pull-down assay. In this assay, N-terminally 6His-tagged SSB (6His-SSB) and un-tagged Redβ were expressed in separate cultures of BL21-AI *E. coli,* and harvested cells were combined prior to sonication to form a mixed-cell lysate that was clarified by centrifugation and loaded onto a Ni-NTA spin column. A positive control shows that 6His-SSB effectively pulls down un-tagged Redβ such that a purified complex elutes with 500 mM imidazole (Figure 7A, top row, lane “E”). By contrast, the individual F171A and F177A mutations in SSB that remove key hydrophobic interactions almost completely disrupt the complex, as little to no band for un-tagged Redβ was present in the respective elutions. The F177A mutation was tested previously with a similar result (18). The I175A mutation in SSB partially disrupts the complex, in concordance with the side chain of I175 being only partially buried at the interface. By contrast, mutations at five residues of SSB that do not make close interactions with the CTD in the complex, including M169A, D172A, D173A, D174A, and P176A have little if any effect on complex formation, as normal bands for un-tagged Redβ were present in the respective elutions. It is particularly noteworthy that the P176A mutation does not destabilize the complex, indicating that proline at this position does not impart any unique conformational properties to SSB-Ct that are required for binding. The lack of effects of P176A and M169A also suggest that the dimer interaction seen in the crystal structures is not important for binding of the full-length proteins, as these residues of SSB (along with Ile-175) form much of the dimer interface. Unexpectedly, D170A results in partial disruption of the complex, despite Asp-170 not forming any close interactions with the CTD in the complex. Although Asp-170 could potentially form long-range electrostatic interactions with the underlying positively charged

surface of the CTD that includes Lys-245 (Figure 2A), the distance of 8.3Å between these residues is too far to account for the disruption of the interaction seen for D170A in the pull down.

Several residues that line the apolar cleft on the Redβ CTD are involved in the interaction with SSB-Ct. We tested seven of them: L223, I227, F228, F249, and L250 that make hydrophobic interactions with F171 and/or F177 of SSB-Ct, and K214 and K253 that make electrostatic interactions with the C-terminal carboxylate and peptide backbone of SSB-Ct, respectively. Mutation of any of these seven residues to alanine significantly disrupts the complex formed by full-length Redβ and SSB proteins (Figure 7B).

Together, the mutational data strongly support the conclusion that the interactions observed in the crystal structure are relevant to the complex formed between the full-length Redβ and SSB proteins in solution. Mutations at residues that make close contacts in the structure significantly disrupt the complex, while nearly all the mutations at residues that don't make substantial contacts have little to no effect (D170A being an exception). All our mutations were to alanine, and thus involved simple removal of side chain interactions as opposed to stronger mutations such as charge reversals or insertions. This suggests a relatively weak association that is sensitive to loss of virtually any of the individual stabilizing interactions, consistent with the moderate affinity of the Redβ–SSB-Ct complex (K_d = 11 μM) measured previously by fluorescence anisotropy (18).

Importantly, none of the mutations significantly altered the expression or solubility of either protein, as similar bands were seen in the whole cell (WC) and soluble (SOL) portions of the cell lysates for each protein variant (Figure 7). This suggests that the mutations do not dramatically alter the folding or solubility of the respective proteins. An advantage of the Ni-spin pull-down method is that it does not require protein purification and thus allows for multiple variants, 16 in our case, to be assessed. The pull-down also mimics cellular conditions as it is performed in the presence of other cellular components from the lysate and at close to physiological ionic strength (50 mM sodium phosphate, 300 mM NaCl, 10-30 mM imidazole, pH 8.0).

Conservation Analysis of the CTD

To determine if the groove on the CTD that is used for binding to SSB-Ct and λ-exo is conserved, we input the CTD amino acid sequence (residues 192-261) into CONSURF server (24) using the default parameters. This generated a multiple sequence alignment of 60 CD-HIT sequences meeting the min/max

similarity criteria. Most of the sequences correspond to CTDs of RecT/Redβ family homologs, suggesting a conserved domain architecture. The resulting multiple sequence alignment is provided as a supplementary html file, and a conservation plot of the structure is shown in Figure 8. The sequences share from 38 – 94 % sequence identity with the CTD of Redβ from bacteriophage λ. Nine of the 70 amino acid residues are invariant in these sequences, including Lys-214 which contacts the C-terminal carboxylate of SSB-Ct, and Lys-245 which does not make direct contacts with SSB-Ct but forms the positively charged surface underneath the carboxylate groups of Asp-170, Asp-172, and Asp-173 of SSB-Ct. The residues that form the apolar DNA binding groove for the two Phe residues of SSB-Ct are in general conserved, but only one of them, Phe-228 at end of the right side of the groove in Figure 8A, is invariant. Two of the invariant residues (Arg-230 and Glu-242) form a close ion pair on the surface of the CTD (on the right as viewed in Figure 8, behind Phe-228), and four of the residues (Pro-222, Leu-221, Trp-216, and Ile-205) form a line of consecutively contacting residues that is predominantly buried in the middle of the structure (partly seen in Figure 8B). Overall, the conservation analysis indicates that the residues lining the groove on the CTD that is used to bind to SSB-Ct and λ-exo are well conserved and thus likely to be used for binding to the equivalent protein partners of RecT/Redβ homologs.

Discussion

As predicted (18), the SSB binding site on the Redβ CTD overlaps extensively with the site for binding of λ-exo. This supports the conclusion that the two interactions cannot occur at the same time (i.e. are mutually exclusive), and further supports a “hand-off” mechanism in which the interaction of Redβ with λ exo helps to load Redβ onto the first ssDNA (Figure 1A), while the interaction of Redβ with SSB helps the initial Redβ–ssDNA complex to access the second ssDNA at the target site of annealing at the lagging strand of a replication fork (Figure 1C). However, we have yet to exclude the possibility of a ternary (Redβ-λ-exo-SSB) complex experimentally. In a previous competition experiment (18), titrating purified Redβ–λ-exo complex into fluorescein-labeled SSB-Ct peptide resulted in some increase in anisotropy (about half of that with Redβ alone), suggesting that the peptide was either displacing Redβ subunits from the λ-exo trimer, or binding to a different site on the 3:3 complex. Further experiments, such as by native MS, will be needed to more fully test the possibility of a ternary complex.

The binding mode observed in the structure is largely consistent with our previous prediction (18), with the C-terminal Phe-177 side chain of SSB inserting into the same pocket on the CTD as Phe-249 of λ-exo. While we also predicted that the C-terminal carboxylate of SSB would be involved in the interaction and form an ion pair with Lys-253, the structure reveals that it instead forms an ion pair with Lys-214. Lys-253 does however reorient to form two interactions with the SSB peptide, a hydrogen bond to the backbone carbonyl of Ile-175, and an ion pair with the carboxylate of Asp-174. The observation that the K253A mutation significantly disrupts the complex observed by Ni-spin pull-down indicates that one or both interactions (with Ile-175 or Asp-174) are important. The fact that the D174A mutation in SSB has minimal effect on the complex suggests that the important interaction is Lys-253 with the backbone carbonyl of Ile-175. This can be rationalized by the structure, as the interaction of Lys-253 with the backbone carbonyl of Ile-175 is closer and more buried.

At least 18 *E. coli* proteins are known to bind to SSB (25-53), many via the SSB C-tail, and structures of at least eight of them have been determined in complex with the same SSB-Ct peptide used in this study (Table 2). Moreover, two other phage proteins, coliphage virion N4 RNA polymerase (54), and recombination mediator Orf from phage λ (55), have been shown to interact with SSB, suggesting that interactions of SSB with many other phage proteins are likely to occur. Interestingly, in all other structures of SSB-Ct bound to an interacting protein, only the last three to five residues of the SSB-Ct peptide are ordered (Table 2). Most of these proteins have different folds and/or binding modes from one another, suggesting that their interactions with SSB have apparently evolved convergently in many instances. In all these structures, binding to the C-terminal Phe-177 residue of SSB is a central feature, both with its side chain and with its C-terminal carboxylate. The interaction with the C-terminal carboxylate often involves a conserved arginine residue that forms a “basic lip”, and many of these proteins also have a “basic ridge” that binds to the carboxylates of D173 and D174 of SSB-Ct. This latter feature is less prominent for our complex of SSB-Ct with Redβ CTD, as the carboxylates of the four aspartate side chains are largely exposed. However, the underlying surface of the CTD, though distant (8-11Å), is positively charged, suggesting that the overall charge complementarity may be important. Most importantly, the complex of the CTD with SSB-Ct involves a prominent interaction with the side chain of Phe-171 of SSB that has not been seen in any of the other complexes. Both the structure and the Ni-Spin pull-down data indicate that the interaction involving Phe-171 is a key feature of the complex. While the involvement of Phe-171 of SSB has

not been observed for any other protein complex, two binding sites for SSB-Ct were observed in the *E. coli* exonuclease I complex, only one of which was deemed functional by mutational analysis (25). As the Phe177 C-α atoms of the two modeled copies of SSB-Ct were only 14.8 Å apart from one another, it is conceivable that the Phe177 residue of the second copy of SSB-Ct could have corresponded to Phe-171 of the first SSB-Ct peptide.

The binding affinities of several proteins for SSB (or SSB-Ct) have been measured and range from 0.1 – 11 μM (Table 2). The affinity of the Redβ–SSB-Ct complex measured by fluorescence polarization (18) is at the low end of this spectrum (11 μM), even though our CTD–SSB-Ct structure includes more ordered residues of SSB-Ct and buries more solvent accessible surface area than any of the other complexes. There may be an entropic penalty for folding the SSB-Ct peptide into the U-shaped conformation observed in the complex with the CTD. Alternatively, the weaker affinity could be due to differences in the methods or buffer conditions used for the various measurements, or from differences in using full-length SSB vs. the SSB-Ct peptide for the measurement.

Some proteins have been suggested to remodel SSB to displace it from the bound ssDNA to gain access to it. For example, PriA was shown to shift SSB from the SSB_{65} into the SSB_{35} binding mode, where larger segments of the ssDNA are exposed (28). This shift in binding mode could occur through sequestering of the SSB C-tail, which removes its interaction with the DNA-binding groove on the SSB core domain and reduces cooperative binding interactions. However, regardless of binding mode, SSB slides along ssDNA by a reptation (bulge formation) mechanism in which all the sequences along the lagging strand would be successively exposed during replication (56). Binding of the initial Redβ-ssDNA complex to SSB at the lagging strand could thus help it to sample the lagging strand sequence until the complementary target site is encountered, at which point Redβ-mediated annealing could occur. In this scenario, Redβ would not need to remodel or displace SSB from the ssDNA, but rather sample the lagging strand sequence as it is exposed during the inherent reptation of SSB along the ssDNA.

The current mutational data indicates that the interaction between Redβ and SSB is mediated largely, if not exclusively, by the CTD of Redβ and the C-tail of SSB. Single point mutations at residues of the CTD or the SSB C-tail at the interface seen in the structure can completely disrupt the complex, as seen by Ni-spin pull-down (Figure 7 and reference 18). Thus, it is likely that the interaction we have captured in the crystal is representative of the interaction that occurs *in vivo*. However, based on the current data we

cannot exclude the possibility that other regions of each protein, such as the NTD of Redβ or the core domain or inter-domain linker (IDL) of SSB are involved in the interaction. In fact, the weak interaction seen for the purified CTD and SSB-Ct by nMS suggests that other interactions or factors may be involved. Moreover, given that SSB is a tetramer and Redβ can also oligomerize, it is intriguing to speculate that multiple CTD–SSB-Ct interactions could occur simultaneously at the lagging strand to increase the avidity of the complex. The shortest oligonucleotide that can be recombined *in vivo* is approximately 20 nucleotides (23). Based on the four bp/monomer observed for Redβ-dsDNA filaments by cryo-EM (57) and the sizes of Redβ-ssDNA complexes detected by nMS (23), a 20-mer oligonucleotide would likely be bound by five copies of Redβ. Thus, the dimer interaction seen in all four crystal forms could still be relevant for the interactions of the full-length Redβ and SSB proteins *in vivo*, despite the lack of dimerization seen for the CTD–SSB-Ct complex by nMS *in vitro*.

The structure of the CTD–SSB-Ct complex reported here may help to explain the differences in efficiency of Redβ-mediated recombination in different bacterial hosts (22). Although the sequence of the SSB-Ct is in general highly conserved, residues further upstream from the C-terminus are more variable. Our work shows that the 7th residue from the end, Phe-171 in the case of *E. coli* SSB, is an important determinant for the interaction of Redβ from bacteriophage λ with *E. coli* SSB. The residue at this position was also shown to be a strong determinant of the efficiency of recombination by orthologs of Redβ in different bacterial hosts (22). It is likely that each Redβ ortholog will contain a CTD with a surface that is optimized for the SSB-Ct of its host SSB protein. Structural analysis of other CTD–SSB-Ct complexes native to other host bacteria will reveal the basis for the specificity of their interactions and guide efforts to optimize recombination efficiency in each host (58).

Materials and Methods

Protein expression and purification

Cloning and purification of the Redβ CTD was as described previously (11). Briefly, the gene corresponding to residues 182-261 of the CTD was cloned into a pET-28b vector for expression of the protein with an N-terminal 6His tag and an intervening site for thrombin cleavage. The protein was expressed in *E. coli* BL21-AI cells, and purified by nickel affinity chromatography (2 x 5 ml Cytiva HisTrap Fast Flow), thrombin

cleavage to remove the 6His tag (Cytiva, product # 27084601), a second pass on the HisTrap column to remove any un-cleaved CTD protein, anion exchange chromatography (Cytiva HiTrap Q Fast Flow), and gel filtration (Cytiva Sephadex S-300) using 20 mM Tris pH 7.5 and 300 mM NaCl as the column running buffer. Pooled fractions from the gel filtration column were concentrated to 27 mg/ml (Vivaspin 20, MWCO 10 kDa) and stored in 100 µl aliquots at -80 °C. The protein concentration was determined by O.D. at 280 nm using the extinction coefficient calculated from the amino acid sequence (6990 M^{-1} cm^{-1}). The final purified protein contains an extra N-terminal Gly-Ser-His-Met sequence from the vector after cleaving with thrombin.

Peptide synthesis

A peptide corresponding to the last nine residues of SSB with an N-terminal tryptophan added for concentration measurement was synthesized by standard Fmoc chemistry, purified by reversed phase HPLC to > 95% homogeneity, authenticated by high-resolution mass spectrometry, and quantified by O.D. at 280 nM (ε = 5500 M^{-1} cm^{-1}). This peptide was used for crystallization and x-ray structure determination. Peptides used for nMS corresponding to the last 9 (MDFDDIPF) or 15 (PSNEPPMDFDDIPF) residues of SSB were purchased from WatsonBio at 4 mg quantity, > 98% purity, lyophilized as TFA salts.

Crystallization and x-ray structure determination

SSB-Ct peptide (white powder) was dissolved in 100% dimethylformamide (DMF) to make a stock concentration of 34 mM, which was stored at -20 °C. For crystallization, an aliquot of purified 13 mg/ml (1.38 mM) Redβ CTD (in 20 mM Tris pH 7.5, 300 mM NaCl) was thawed, and 76.9 µl was mixed with 5.0 µl of 34 mM SSB-Ct peptide (in DMF). Slight precipitation, presumably of the SSB-Ct peptide, was observed but disappeared upon mixing. The complex was then diluted by adding 18.1 µl of ddH_2O to result in a final complex of 10 mg/ml (1.1 mM) Redβ CTD and 1.7 mM SSB-Ct peptide. Crystal screens were performed in 96-well hanging drop format using a Mosquito instrument. Hanging drops contained 0.2 µl of complex and 0.2 µl of cocktail solution and were hung over 100 µl of cocktail solution. Cocktail solutions were from standard commercial crystal screens from Hampton Research and Molecular Dimensions. Crystals grew from several different conditions, all of which contained high concentrations of salt as the main precipitating agent. After optimization in 24-well plates with 2 µl + 2 µl hanging drops and 1 ml of well solution, Form 1 crystals grew from 0.48 M sodium phosphate monobasic monohydrate, 1.2 M potassium phosphate dibasic,

pH 7.2, and were transferred into the same solution supplemented with 30% glycerol as cryoprotectant. Form 2 crystals grew from 2.0 M ammonium sulfate, 0.1 M Tris pH 8.6, and were transferred into 2.2 M ammonium sulfate, 0.1 M Tris pH 8.6, 30% glycerol as cryoprotectant. Form 3 crystals grew from 1.2 M sodium citrate tribasic dihydrate, 0.1 M Tris pH 8.6, and were transferred into 1.5 M sodium citrate tribasic dehydrate, 0.1 M Tris pH 8.6, 30% glycerol as cryoprotectant. Form 4 crystals grew from 2.4 M ammonium phosphate dibasic, 0.1 M Tris pH 8.5, and were transferred into 3.0 M ammonium phosphate dibasic and 20% glycerol as cryoprotectant. All crystals were mounted in nylon loops (Hampton Research) and plunge-frozen in liquid nitrogen.

X-ray diffraction data were collected at Beamline 31-ID of the Advanced Photon Source at Argonne National laboratory. Images were processed with an automatic workflow consisting of autoPROC version 1.1.7 (59), XDS (60) (version Jan 26, 2018, BUILT 20180808), POINTLESS version 1.11.21 (61), AIMLESS version 0.7.4 (62), CCP4 version 7.0.075 (63), and STARANISO version 2.3.28 (64). The final anisotropic (ellipsoidal) reduced data sets were used for structure determination and crystallographic refinement. The Form 1 structure was determined by molecular replacement (MOLREP version 11.4.03 (65)) using a single chain (monomer) of the structure of the Redβ CTD determined in complex with λ exo as a starting model (PDB accession code 6M9K). After the first round of refinement (REFMAC5 version 5.8.0267 (66)), clear density for all ten residues of the peptide was observed, and a model for the peptide was built using COOT (67). Multiple rounds of model adjustment and addition of water molecules in COOT, alternating with refinement in REFMAC5, resulted in a final model with R and free R values of 18.4 and 22.4%, respectively. Forms 2, 3, and 4 were determined by molecular replacement using the Form 1 structure as a starting model and re-built and refined as described for Form 1. Full data collection and refinement statistics are provided in Table 1. Solvent accessible surface areas buried upon complex formation were calculated using AREAIMOL version 7.1.018 with a probe radius of 1.4Å. Structural figures were generated using PyMOL (68).

Nickel-Spin Pull-Down Assay

Ni-spin pull-down assays were performed as described previously (18). Briefly, Redβ with its native (un-tagged) sequence was expressed from pET-9a, and 6His-SSB was expressed from pET-28b, in separate 50 ml cultures of BL21-AI *E. coli* cells (Invitrogen). The indicated mutations in Redβ and 6His-SSB were

introduced into each vector using the QuikChange method (Agilent Technologies) and confirmed by Sanger di-deoxy DNA sequencing. After induction with 0.2% arabinose and 1 mM IPTG for four hours, cells were harvested by centrifugation, re-suspended in 3.0 ml of Sonication Buffer (50 mM NaH_2PO_4, 300 mM NaCl, 10 mM imidazole), and frozen at -80 °C. Thawed cells, 1.5 ml each of Redβ and 6His-SSB, were mixed, incubated for 60 min with 1 mg/ml lysozyme and protease inhibitors (leupeptin, pepstatin, and PMSF), lysed by sonication, and centrifuged at 38,000 x g. The clarified supernatants were loaded onto Ni-NTA spin columns (Qiagen), washed (4 x 500 µl) with Sonication Buffer containing 30 mM imidazole, and eluted (2 x 200 µl) with buffer containing 500 mM imidazole. Fractions analyzed by SDS-PAGE included whole cell lysate (WC), soluble portion of the lysate after centrifugation (SOL), the first and fourth washes with 30 mM imidazole (W1 and W4), and the first elution with 500 mM imidazole (E).

Native Mass Spectrometry

nMS experiments were performed on a Q Exactive Ultra-High Mass Range (UHMR) orbitrap mass spectrometer from Thermo Fisher that was modified with a 4-cm 12 lens for surface-induced dissociation (SID, not used in this work; 69). Redβ CTD protein was prepared by buffer exchange into 200 mM ammonium acetate pH 7 (unadjusted) using a Pierce 96-well microdialysis plate with a 3.5K MWCO (Thermo Fisher). Both SSB-Ct 9-mer and 15-mer peptide were dissolved in ddH_2O. CTD was diluted at the indicated concentration into 200 mM ammonium acetate pH 7 (unadjusted). For the preparation of CTD–SSB-Ct complexes, CTD was first mixed with SSB-Ct peptide at the concentration used for growing crystals (1.06 mM CTD, 1.7 mM SSB-Ct) and then diluted to the indicated final concentration in 800 mM ammonium acetate. Each sample was injected into an in-house pulled borosilicate filament capillary (OD 1.0 mm, ID 0.78 mm) and subsequently ionized by nano-electrospray ionization. The instrument tuning settings were as follows: capillary temperature 250°C, Source DC Offset 21 V, S-lens RF level 200, detector m/z optimization low m/z, noise threshold 4.64, ion transmission target low m/z. The low m/z transmission includes the following settings: Injection flatapole RF amplitude 150, bent flatapole RF amplitude 300, Transfer multiple and HCD-cell RF amplitudes 250, and C-trap RF amplitude 2300. Other instruments settings include as follows: injection flatapole DC 5 V, inter flatapole lens 4 V, bent flatapole DC 2 V, Transfer multipole DC 0 V, C-trap entrance lens inject 1.8 V, HCD field gradient 200 V, HCD cell pressure 1 (UHV sensor 7E-11~1E-10 mbar), and resolution 6,250 for protein alone while 3,125 and 50,000 for the complexes as defined at 400

m/z. The spray voltage was adjusted between 0.5 and 0.8 kV and held constant for the acquisition duration. Ion activation was necessary for improved transmission and de-adducting of ions. This activation via in-source trapping (IST) of -5 V was used.

All data were deconvolved using UniDec V6.0.3 (70). The deconvolution settings used for CTD alone included the following: m/z range 1250–3000, charge range 1–15, mass range 7–21 kDa, sample mass every 1 Da, split Gaussian/Lorentzian peak FWHM 0.7 Th, charge smooth width 1.0. The deconvolution settings used for the CTD–SSB-Ct complex included the following: m/z range 1250–3000, charge range 1–6, mass range 8–13 kDa, sample mass every 1 Da, split Gaussian/Lorentzian peak FWHM 0.1 Th, charge smooth width 1.0.

Acknowledgements

The authors thank Dr. Dehua Pei and Dr. Curran Rhodes at The Ohio State University Department of Chemistry and Biochemistry for providing the 10-mer SSB-Ct peptide used for co-crystallization. This work was funded by grants from the National Science Foundation (MCB-1616105 and MCB-2212951 to C.E.B) and the National Institutes of Health (T32GM11829 to B.J.C. and P41GM128577 and RM1GM149374 to V.H.W). The content is solely the responsibility of the authors and does not necessarily represent the official views of the National Science Foundation or the National Institutes of Health.

References

1. Kmiec, E., Holloman, W.K. (1981). β protein of bacteriophage λ promotes renaturation of DNA. *J. Biol. Chem.* **256**, 12636–12639.
2. Muniyappa, K., Radding,C.M. (1986). The homologous recombination system of phage λ. Pairing activities of β protein. *J. Biol. Chem.* **261**, 7472–7478
3. Vellani, T.S. Myers, R.S. (2003). Bacteriophage SPP1 Chu is an alkaline exonuclease in the SynExo family of viral two-component recombinases. *J. Bacteriol.* 1**85**, 2465–2474.
4. Caldwell, B.J. and Bell, C.E. (2019). Structure and mechanism of the Red recombination system of bacteriophage λ. *Prog. Biophys. Mol. Biol.* **147**, 33–46.
5. Little,J.W. (1967). An exonuclease induced by bacteriophage λ II. Nature of the enzymatic reaction. *J. Biol. Chem.* **242**, 679–686.
6. Kovall, R., Matthews, B.W. (1997). Toroidal structure of λ-exonuclease. *Science* **277**, 1824–1827.
7. Zhang, J., McCabe, K. A., Bell, C.E. (2011). Crystal structures of λ exonuclease in complex with DNA

suggest an electrostatic ratchet mechanism for processivity. *Proc. Natl. Acad. Sci. USA* **108**, 11872–11877.

8. Radding, C.M., Rosenweig, J., Richards, F., Cassuto, E. (1971). Separation and characterization of exonuclease, β protein, and a complex of both. *J. Biol. Chem.* **246**, 2510–2512.
9. Muyrers, J.P.P., Zhang, Y., Buchholz, F., Stewart, A.F. (2000). RecE/RecT and Redα/Redβ initiate double-stranded break repair by specifically interacting with their respective partners. *Genes Dev.* **14**, 1971–1982.
10. Wu, Z., Xing, X., Wisler, J.W., Dalton, J.T., Bell, C. E. (2006). Domain structure and DNA binding regions of β protein from bacteriophage λ. *J. Biol. Chem.* **281**, 25205–25214.
11. Smith, C.E., Bell, C.E. (2016). Domain structure of the Redβ single-strand annealing protein: the C-terminal domain is required for fine-tuning DNA-binding properties, interaction with the exonuclease partner, and recombination in vivo. *J. Mol. Biol.* **428**, 561–578.
12. Datta, S., Costantino, N., Zhou, X., Court, D.L. (2008). Identification and analysis of recombineering functions from Gram-negative and Gram-positive bacteria and their phages. *Proc. Natl. Acad. Sci. U.S.A.* **105**, 1626–1631.
13. Zhang, Y., Buckholz, F., Muyrers, J.P.P., Stewart, A.F. (1998). A new logic for DNA engineering using recombination in *Escherichia coli*. *Nat. Genet*. **20**, 123–128.
14. Copeland, N.G., Jenkins, N.A. Court, D.L. (2001). Recombineering: A powerful new tool for mouse functional genomics. *Nat. Rev. Genet*. **2**, 769–779.
15. Wang, H.H., Isaacs, F.J., Carr, P.A., Sun, Z.Z., Xu, G., Forest, C.R., Church, G.M. (2009) Programming cells by multiplex genome engineering and accelerated evolution. *Nature* **460**, 894–898.
16. Zhang, Y., Muyrers, J.P., Rientjes, J., Stewart, A.F. (2003) Phage annealing proteins promote oligonucleotide-directed mutagenesis in *Escherichia coli* and mouse ES cells. *BMC Mol. Biol.* **4**, 1.
17. Ellis, H.M., Yu, D., DiTizio, T., Court, D.L. (2001). High efficiency mutagenesis, repair, and engineering of chromosomal DNA using single-stranded oligonucleotides. *Proc. Natl. Acad. Sci. USA*, **98**, 6742–6746.
18. Caldwell, B.J., Zakharova, E., Filsinger, G.T., Wannier, T.M., Hempfling, J.P., Chun-Der, L., Pei,D., Church, G.M., Bell, C.E. (2019). Crystal structure of the Redβ C-terminal domain in complex with λ exonuclease reveals and unexpected homology with λ Orf and an interaction with *Escherichia coli* single-stranded DNA binding protein. *Nucleic Acids Res.*, **47**, 1950–1963.
19. Curth, U., Genschel, J., Urbanke, C., Greipel, J. (1996). *In vitro* and *in vivo* function of the C-terminus of *Escherichia coli* single-stranded DNA binding protein. *Nucleic Acids Res.*, **24,** 2706–2711.
20. Shereda, R.D., Kozlov,A.G., Lohman,T.M., Cox,M.M. and Keck,J.L. (2008). SSB as an organizer/mobilizer of genome maintenance complexes. *Crit. Rev. Biochem. Mol. Biol.*, **43,** 289–318.
21. Costes, A., Lecointe, F., McGovern, S., Quevillon-Cheruel, S., Polard, P. (2010). The C-terminal domain of the bacterial SSB protein acts as a DNA maintenance hub at active chromosome replication forks. *PLoS Genet.*, **6**, e1001238.
22. Filsinger, G.T., Wannier T.M., Pedersen, F.B., Lutz, I,D,, Zhang, J, Stork,D.A. et al. (2021).

Characterizing the portability of phage-encoded homologous recombination proteins. *Nature Chem. Biol.*, **17**, 394–402.

23. Caldwell, B.J., Norris, A., Zakharova, E., Smith, C.E., Wheat, C.T, Choudhary, D., Sotomayor, M., Wysocki, V.H. (2021). Oligomeric complexes formed by Redβ single strand annealing protein in its different DNA bound states. *Nucleic Acids Res.* **49**, 3441–3460.
24. Ashkenazy, H., Abadi, S., Martz, E., Chay, O., Mayrose, I., Pupko, T., Ben-Tal, N. (2016). ConSurf 2016: an improved methodology to estimate and visualize evolutionary conservation in macromolecules. *Nucleic Acids Res.* **44**, W344–W350.
25. Lu, D., and Keck, J. L. (2008). Structural basis of *Escherichia coli* single-stranded DNA-binding protein stimulation of exonuclease I. *Proc. Natl. Acad. Sci. U.S.A.* **105,** 9169–9174.
26. Ryzhikov, M., Koroleva, O., Postnov, D., Tran, A., and Korolev, S. (2011). Mechanism of RecO recruitment to DNA by single-stranded DNA binding protein. *Nucleic Acids Res.* **39,** 6305–6314.
27. Shinn, M.K., Kozlov, A.G., Nguyen, B., Bujalowski, W.M. Lohman, T.M. (2019). Are the intrinsically disordered linkers involved in SSB binding to accessory proteins? *Nucleic Acids Res.*, **47**, 8581–8594.
28. Bhattacharyya, B., George, N.P, Thurmes, T.M., Zhour, R., Jani, N., Wessel, S.R., Sandler, S.J., Ha, T., Keck, J.L. (2013). Structural mechanisms of PriA-mediated DNA replication restart. *Proc. Natl. Acad. Sci. USA* **111**, 1373–1378.
29. Cadman CJ, McGlynn P (2004). PriA helicase and SSB interact physically and functionally. *Nucleic Acids Res.* **32**, 6378–6387.
30. Marceau, A.H., Bahng, S., Massoni, S.C., George, N.P., Sandler, S.J., Marians, K.J., Keck, J.L. (2011). Structure of the SSB-DNA polymerase III interface and its role in DNA replication. *EMBO J.* **30,** 4236–4247.
31. Witte, G., Urbanke, C., Curth, U. (2003). DNA polymerase III chi subunit ties single-stranded DNA binding protein to the bacterial replication machinery. *Nucleic Acids Res.* **31**, 4434-4440.
32. Glover, B.P., McHenry C.S. (1998). The ChiPsi subunits of DNA Polymerase II Holoenzyme bind to SSB and Facilitate Replication of an SSB-coated Template. *J. Biol. Chem.* **273**, 23476–23484.
33. Kelman et al. (1998). Devoted to the lagging strand–the chi subunit of DNA polymerase III holoenzyme contacts SSB to promote processive elongation and sliding clamp assembly. *EMBO J.* **17**, 2436–2449.
34. Yuzhakov et al. (1999). Trading Places on DNA- A Three-Point switch underlies primer handoff from primase to the replicative DNA polymerase. *Cell* **96**, 153–163.
35. Petzold, C., Marceau, A.H., Miller, K.H., Marqusee, S., Keck, J.L. (2015). Interaction with single-stranded DNA-binding protein stimulates *Escherichia coli* ribonuclease HI enzymatic activity. *J. Biol. Chem.* **290**, 14626–14636.
36. Cheng, K., Xu, H., Chen, X., Wang, L., Tian, B., Zhao, Y. and Hua, Y. (2016). Structural basis for DNA 5'-end resection by RecJ. *Elife* **5**, e14294.
37. Purnapatre K, Handa, P., Venkatesh, J., Varshney, U. (1999) Differential effects of single-stranded DNA binding proteins (SSBs) on uracil DNA glycosylases (UDGs) from Escherichia coli and mycobacteria. *Nucleic Acids Res.* **27**, 3487–3492.

38. Naue, N., Beerbaum, M., Bogutzki, A., Schmieder P, Curth, U. (2013). The helicase-binding domain of Escherichia coli DnaG primase interacts with the highly conserved C-terminal region of single-stranded DNA-binding protein. *Nucleic Acids Res.* **41**, 4507–4517.
39. Wessel, S.R., Marceau, A.H., Massoni, S.C., Zhou, R., Ha, T., Sandler, S.J. and Keck, J.L. (2013) PriC-mediated DNA replication restart requires PriC complex formation with the single-stranded DNA-binding protein. *J. Biol. Chem.* **288**, 17569–17578.
40. Shereda, R.D., Reiter, N.J., Butcher, S.E., Keck, J.L. (2009). Identification of the SSB binding site on *E. coli* RecQ reveals a conserved surface for binding SSB's C terminus. *J. Mol. Biol.* **386,** 612– 625.
41. Shereda, R.D. et al. (2007). A central role for SSB in Escherichia coli RecQ DNA helicase function. *J. Biol. Chem.* **282**, 19247–19258.
42. Page, A.N., George, N.P., Marceau, A., Cox, M.M., Keck, J.L. (2011). Structure and Biochemical Activities of *Escherichia coli* MgsA. *J. Biol. Chem.* **286**, 12075–12085.
43. Chang, S., Thrall, E.S., Laureti, L., Piatt, S.C., Pagés, V., Loparo, J.J. (2022). Compartmentalization of the replication fork by single-stranded DNA-binding protein regulates translesion synthesis. *Nat. Struct. Mol. Biol.* **29**, 932–9941.
44. Furukohri, A., Nishikawa, Y., Akiyama, M.T., Maki, H. (2012). Interaction between *Escherichia coli* DNA polymerase IV and single-stranded DNA-binding protein is required for DNA synthesis on SSB-coated DNA. *Nucleic Acids Res.* **40**, 6039–6048.
45. Osorio Garcia, M.A., Wood, E.A., Keck, J.L., Cox, M.M. (2023). Interaction with single-stranded DNA-binding protein modulates *Escherichia coli* RadD DNA repair activities. *J. Biol. Chem.* **299**, 104774.
46. Chen, S.H., Byrne-Nash, R.T., Cox, M.M. (2016). *Escherichia coli* RadD protein functionally interacts with the single-stranded DNA-binding protein. *J. Biol. Chem.* **291**, 20779–20786.
47. Bonde, N.J., Henry, C., Wood, E.A., Cox, M.M., Keck, J.L. (2023). Interaction with the carboxy-terminal tip of SSB is critical for RecG function in E. coli. *Nucleic Acids Res.* **51**, 3735–3753.
48. Ding, W., Tan, H.Y., Zhang, J.X., Wilczek, L.A., Hsieh, K., Mulkin, J.A., Bianco, P.R. (2020). The mechanism of single strand binding protein–RecG binding: implications for SSB interactome function. *Protein Science* **29**, 1211–1227.
49. Nigam, R., Mohan, M., Shivange, G., Dewangan, P.K. and Anindya, R. (2018) *Escherichia coli* AlkB interacts with single-stranded DNA binding protein SSB by an intrinsically disordered region of SSB. *Mol. Biol. Rep.* **45**, 865–870.
50. Cheng, Z., Caillet, A., Ren, B., Deng, H. (2012). Stimulation of *Escherichia coli* DNA damage inducible DNA helicase DinG by the single-stranded DNA binding protein SSB. *FEBS Letters* **586**, 3825–3830.
51. Butland G, Peregrin-Alvarez JM, Li J, Yang W, Yang X, Canadien V, Starostine A, Richards D, Beattie B, Krogan N, Davey M, Parkinson J, Greenblatt J, Emili A. 2005. Interaction network containing conserved and essential protein complexes in *Escherichia coli*. *Nature,* **433**, 531–537.
52. Suski, C., Marians, K.J. (2008). Resolution of converging replication forks by RecQ and topoisomerase III. *Mol. Cell* **30**, 779–789.
53. Arad, G., Hendel, A., Urbanke, C., Curth, U., Livneh, Z. (2008). Single-stranded DNA-binding protein

recruits DNA polymerase V to primer termini on RecA-coated DNA. *J. Biol. Chem.* **283**, 8274-8284.
54. Davydova, E.K., Rothman-Denes, L.B. (2003). *Escherichia coli* single-stranded DNA-binding protein mediates template recycling during transcription by bacteriophage N4 virion RNA polymerase. *Proc. Natl. Acad. Sci. U.S.A.* **100**, 9250-9255.
55. Maxwell, K.L, Reed, P., Zhang, R.G., Beasley, S., Walmsley, A.R., Curtis, F.A., Joachimiak, A., Edwards, A.M., and Sharples, G.J. (2005) Functional similarities between phage λ Orf and Escherichia coli RecFOR in initiation of genetic exchange. *Proc. Natl. Acad. Sci. U.S.A.*, **102**, 11260–11265.
56. Zhour, R., Kozlov, A.G., Roy, R., Zhang, J., Korolev, S., Lohman, T.M., Ha, T. (2011). SSB functions as a sliding platform that migrates on DNA via reptation. *Cell* **146**, 222-232.
57. Newing, T.P., Brewster, J.L., Fitschen, L.J., Bouwer, J.C., Johnston, N.P., Yu, H., Tolun, G. (2022). Redβ$_{177}$ annealase structure reveals details of oligomerization and λ Red-mediated homologous DNA recombination. *Nat. Commun.* **13**, 5649.
58. Asin-Garcia, E., Garcia-Morales, L., Bartholet, T., Liang, Z., Isaacs, F.J., Martins dos Santos, V.A.B. (2023). Metagenomics harvested genus-specific single-stranded DNA-annealing proteins improve and expand recombineering in *Pseudomonas* species. *Nucleic Acids Res.* **51**, 12522–12536.
59. Vonrhein, C., Flensburg, C., Keller, P., Sharff, A., Smart, O., Paciorek, W., Womack, T., Bricogne, G. (2011). Data processing and analysis with the autoPROC toolbox. *Acta Cryst.* **D67**, 293–302.
60. Kabsch, W. (2010). XDS. *Acta Cryst.* **D66**, 125–132.
61. Evans,P.R. (2006). Scaling and assessment of data quality. *Acta Cryst.* **D62**, 72–82.
62. Evans,P.R., Murshudov,G.N. (2013). How good are my data and what is the resolution? *Acta Cryst.* **D69**, 1204–1214.
63. Winn, M.D., Ballard, C.C., Cowtan, K.D. Dodson, E.J., Emsley, P., Evans, P.R., Keegan, R.M., Krissinel, E.B., Leslie, A.G.W., McCoy, A., McNicholas, S.J., Murshudov, G.N., Pannu, N.S., Potterton, E.A., Powell, H.R., Read, R.J., Vagin, A. and Wilson, K.S. (2011). Overview of the CCP4 suite and current developments. *Acta. Cryst.* **D67**, 235–242.
64. Tickle, I.J., Flensburg, C., Keller, P., Paciorek, W., Sharff, A., Vonrhein, C., Bricogne, G. (2020). STARANISO. Cambridge, United Kingdom: Global Phasing Ltd.
65. Vagin, A., Teplyakov, A. (1997). MOLREP: an automated program for molecular replacement. *J. Appl. Cyrst.* **30**, 1022–1025.
66. Kovalevskiy, O., Nicholls, R.A., Long, F., Murshudov, G.N. (2018). Overview of refinement procedures within REFMAC5: utilizing data from different sources. *Acta Crystallogr.* **D74**, 492–505.
67. Emsley, P., Cowtan,K . (2004). Coot: model-building tools for molecular graphics. *Acta Crystallogr. D* **60,** 2126–2132.
68. Delano, W.L. (2002). *The PyMOL Molecular Graphics System*, Schrödinger, LLC, New York.
69. VanAernum, Z.L., Gilbert, J.D., Belov, M., Makarov, A.A., Horning, S.R. and Wysocki, V.H. (2019). Surface-induced dissociation of noncovalent protein complexes in an extended mass range orbitrap mass spectrometer. *Anal. Chem.* **91**, 3611–3618.
70. Marty, M.T., Baldwin, A.J., Marklund, E.G., Hochberg, G.K.A., Benesch, J.L.P., Robinson, C.V. (2014).

Bayesian deconvolution of mass and ion mobility spectra: From binary interactions to polydisperse ensembles. *Anal. Chem.* **87**, 4370–4376.

Table 1. X-ray data collection and structure determination statistics.

	Form 1 (Na/K PO_4)	**Form 2 ($[NH_4]_2[SO_4]$)**	**Form 3 (Na citrate)**	**Form 4 ($[NH_4]_2[PO_4]$)**
PDB	8TFU	8TG7	8TG8	8TGC
Data Collection				
Wavelength (Å)	0.97930	0.97930	0.97930	0.97931
Resolution range (high bin) (Å)	1.48 - 35.44 (1.48 - 1.59)	1.78 - 49.41 (1.78 - 1.89)	1.58 - 49.53 (1.58 - 1.68)	1.48 - 35.64 (1.48 - 1.64)
Space Group	P212121	P212121	P41212	P212121
Unit Cell				
a, b, c (Å)	37.8, 68.3, 70.9	38.3, 69.2, 70.5	70.0, 70.0, 38.4	37.6, 67.9, 71.3
α, β, γ (°)	90, 90, 90	90, 90, 90	90, 90, 90	90, 90, 90
Completeness-ellipsoidal (high bin) (%)	91.9 (52.5)	92.8 (41.8)	91.1 (40.9)	85.1 (52.5)
Completeness-spherical (high bin) (%)	80.1 (21.2)	86.5 (25.5)	84.6 (24.3)	63.3 (12.2)
Unique reflections/total	25,018 / 154,349	16,243 / 101,937	11,588 / 141,963	19,557 / 109,757
Multiplicity	6.2 (6.1)	6.3 (6.8)	12.3 (11.8)	5.6 (3.1)
$I/\sigma I$	14.1(1.2)	15.1 (1.3)	18.8 (1.2)	13.4 (1.4)
R_{merge} (all I+ & I-) (%)	0.062 (1.22)	0.055 (1.40)	0.054 (2.12)	0.074 (0.699)
Rpim (all I+ & I-) (%)	0.027 (0.526)	0.024 (0.576)	0.022 (0.857)	0.033 (0.475)
Refinement				
Resolution (Å)	1.48 - 34.15	1.77 - 49.41	1.58 - 49.53	1.48 - 35.66
CTD Subunits per A.U.	2	2	1	2
R_{work}/R_{free} (%)	18.4 / 22.4	18.4 / 23.8	20.5 / 23.8	20.4 / 26.0
r.m.s. deviations				
Bonds	0.012	0.011	0.011	0.009
Angles	1.7	1.6	1.7	1.6
Ramachandran Stats				
Favored (%)	98.7	97.2	97.3	98.7
Allowed (%)	1.3	2.8	2.7	1.3
Disallowed (%)	0	0	0	0
No. atoms	1,405	1,323	654	1,469
Protein	1,074	1,040	516	1,074
Peptide	184	184	92	184
Water	147	99	46	211
Mean B Factors ($Å^2$)				
Protein	31.0	42.2	46.7	22.9
Peptide	46.5	54.7	63.0	37.9
Water	44.4	55.2	55.9	36.4

Table 2. Known SSB binding partners, structures of complexes, and affinity of interaction.

SSB-interacting Protein	Structure		Affinity Measurement	Qualitative Interaction
	(PDB)	SSB-Ct residues ordered		
Exonuclease I	3C94 [25]	DIPF	136 nM [25]	
RecO	3Q8D [26]	IPF	60-340 nM [26]; 83-323 nM [27]	
PriA helicase	4NL8 [28]	DDIPF	3.8 μM [27]; 2.4-6.9 μM [29]	
DNA Pol III (Chi)	3SXU [30]	DIPF	8.9-9.9 μM [30]	[31-34]
RNase HI	4Z0U [35]	DIPF	2.0 μM [35]	
RecJ	5F56 [36]	ADLPF		
UDG	3UF7 (2011)	DIPF	0.17 μM [37]	
DnaG Primase	6CBR, 6CBS, 6CBT (2018)	DDIPF	11-14 μM [38]	
PriC			625 nM [39]; 3.7 μM [27]	
RecQ			6 μM [40]	[41]
MgsA			360 nM [42]	
DNA Pol IV			2 μM [43]	[44]
RadD			5.4 μM [45]	[46]
RecG			2.6-3.9 μM [47]	[48]
AlkB				[49]
DinG				[50]
Topo III				[51,52]
DNA Pol V				[53]
N4 RNA Pol				[54]
Phage λ Orf				[55]

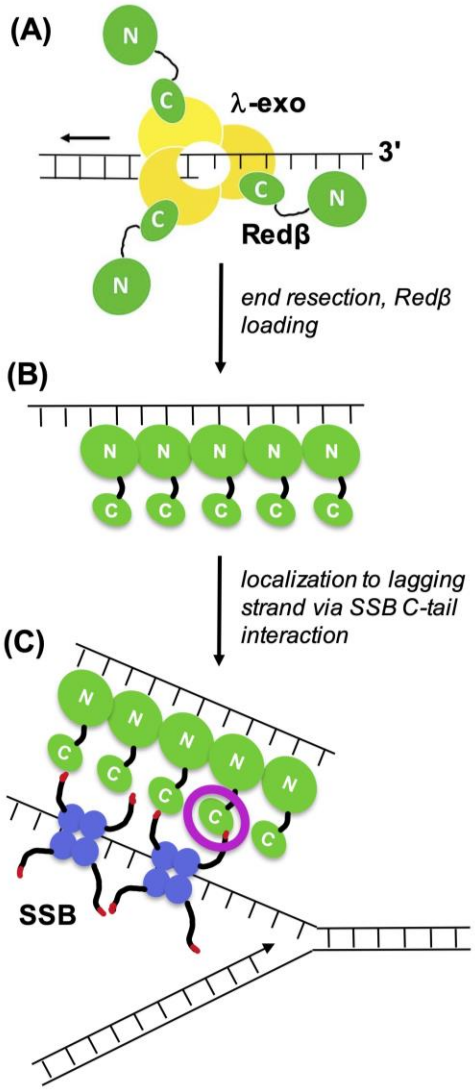

Figure 1. **Overview of protein-protein interactions involved in Red recombination**. (**A**) The λ-exo trimer (yellow) binds to double stranded DNA ends and processively digests the 5'-strand to form a 3'-overhang. An interaction with the CTD loads Redβ directly onto the ssDNA as it is formed by λ-exo. (**B**) Redβ forms an oligomeric complex on ssDNA via it's N-terminal DNA binding domain. A similar type of complex can form on an electroporated oligonucleotide, without involvement of λ-exo (16, 17) (**C**) An interaction of the CTD with the C-terminal tail of SSB (red tip at the end of the black tail) brings the Redβ-ssDNA complex to the replication fork, where it can scan the lagging strand for a complementary sequence to anneal with. The magenta circle indicates the crystallized complex containing the CTD and the SSB C-tail peptide.

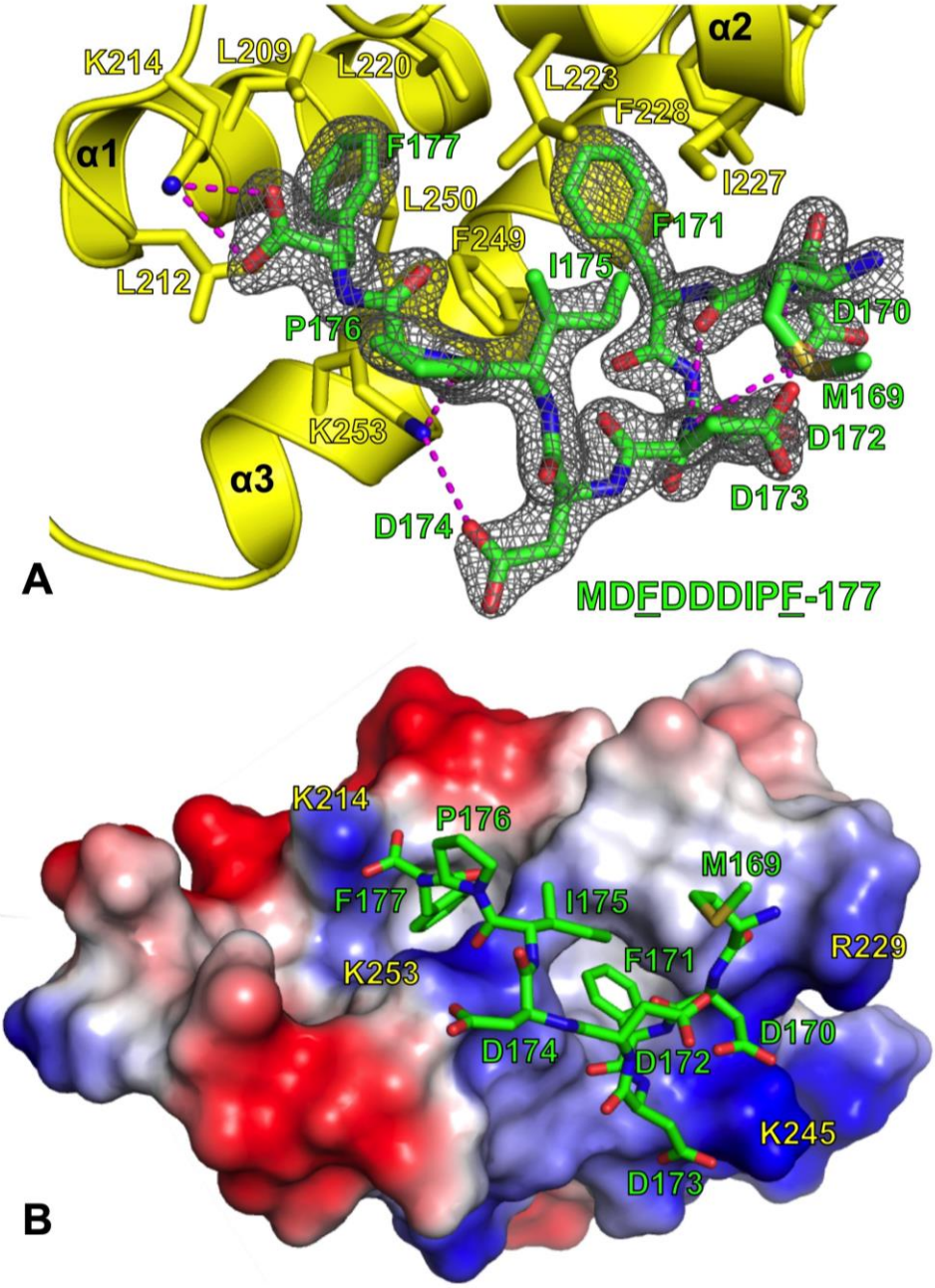

Figure 2. **Structure of the Redβ CTD in complex with SSB-Ct peptide**. (**A**) View of the complex with the CTD in yellow ribbon and the SSB-Ct peptide in green. Hydrogen bonds within 3.7Å are shown as dashed magenta lines. The 1.5Å resolution 2Fo-Fc electron density map is contoured around the peptide in grey mesh. The sequence of the SSB-Ct peptide is shown below the structure with the two key phenylalanine residues underlined. (**B**) Electrostatic molecular surface view of the CTD with positively charged regions in blue and negatively charged regions in red. Notice that the side chains of Phe-171 and Phe-177 of SSB-Ct insert deeply into two adjacent apolar pockets on the CTD. Also notice that the four negatively charged aspartate residues and C-terminal carboxylate of SSB-Ct form potentially favorable electrostatic interactions with positively charged residues of the CTD (labeled in yellow).

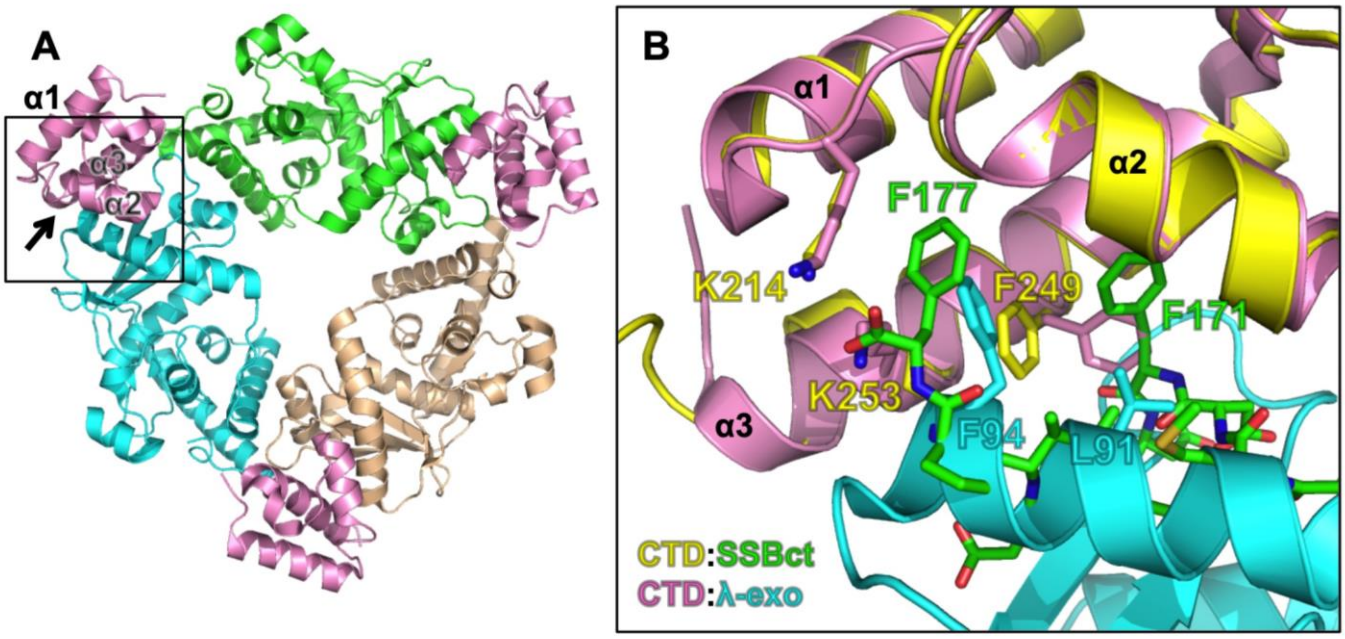

Figure 3. **Structural comparison of the complexes of Redβ CTD with SSB-Ct and λ-exo**. (**A**) Structure of the λ-exo trimer (subunits in green, cyan, and wheat) in complex with three copies of Redβ CTD (pink). Each CTD contacts only one λ-exo subunit at a time (as indicated by the arrow). Structural coordinates are from PDB ID 6M9K (18). (**B**) Superposition of the CTD bound to SSB-Ct (yellow and green) and to the λ-exo trimer (pink and cyan). The close-up view is of the boxed region in panel A from the direction indicated by the arrow in panel A. The SSB-Ct peptide is shown with all side chains in green. Selected side chains of the CTD and λ-exo are shown. Notice that Phe-249 of the CTD adopts different orientations to accommodate Phe-171 of SSB-Ct (yellow side chain) or Phe-94 of λ-exo (pink side chain). Phe-177 of SSB-Ct binds to approximately the same pocket on the CTD as Phe-94 of λ-exo, while Phe-171 of SSB-Ct plugs into a new pocket on the CTD formed by the re-orientation of Phe-249.

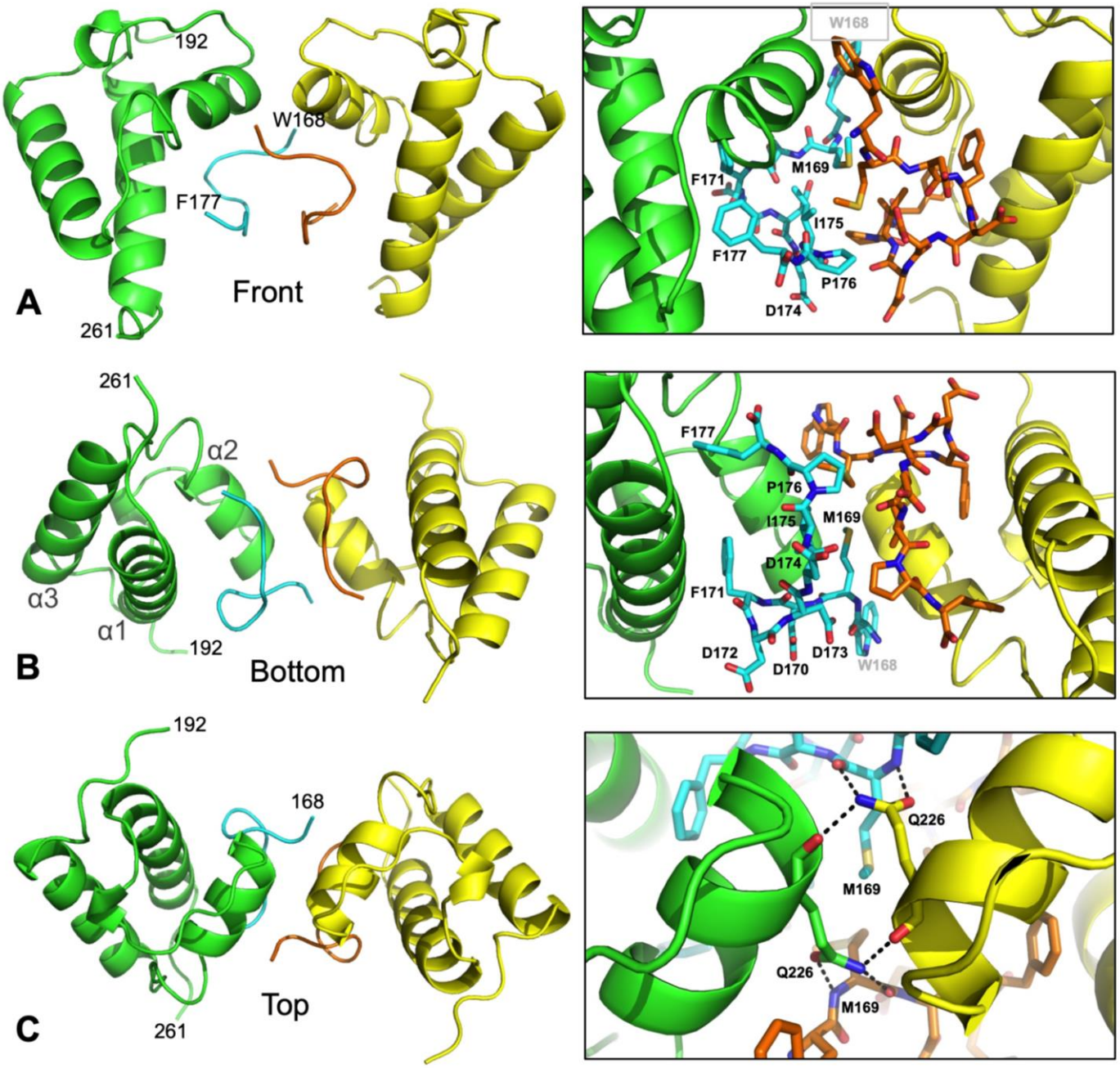

Figure 4. **Structure of the Redβ CTD–SSB-Ct dimer**. The three panels show three different orientations of the dimer: (**A**) Front, (**B**) Bottom, (**C**) Top. The boxed panels to the right show close-up view in each orientation with side chain interactions shown in stick form. A network of hydrogen bonds involving Gln-226 of each CTD is shown in dashed lines in panel C. The views in panels B and C are looking down the 2-fold axis from the bottom and top, respectively.

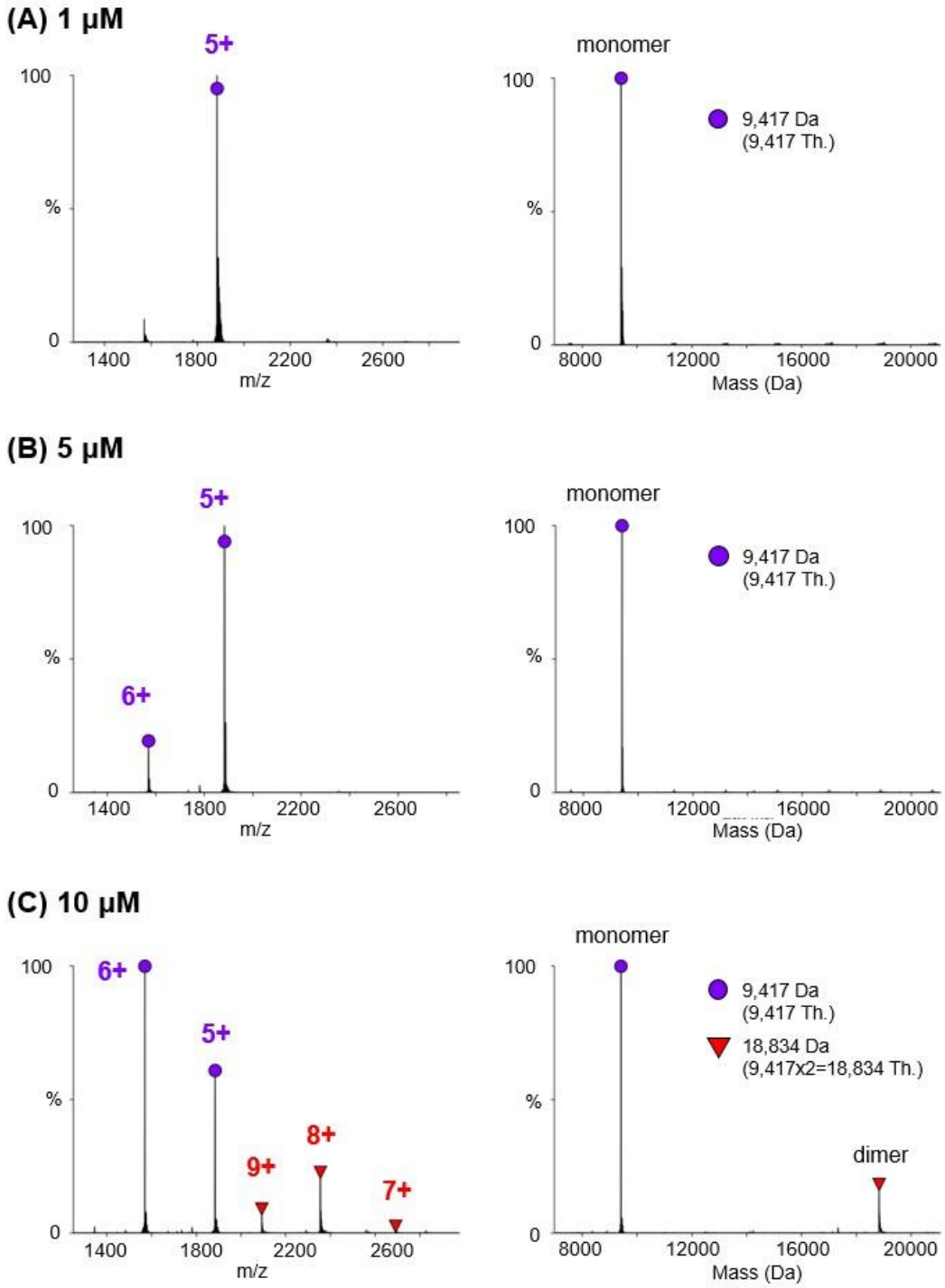

Figure 5. nMS of Redβ CTD. CTD protein was dialyzed into 200 mM ammonium acetate pH 7.0 and analyzed by nMS with the following settings: R6k, IST30, TG1, low ion transmission. Notice that the CTD is fully monomeric at 1 and 5 µM, while some dimer is formed at 10 µM, possibly due to non-specific binding when high concentrations of CTD are present in a single droplet. The experiments shown are representative of multiple experiments under different conditions, which all lead to similar conclusions.

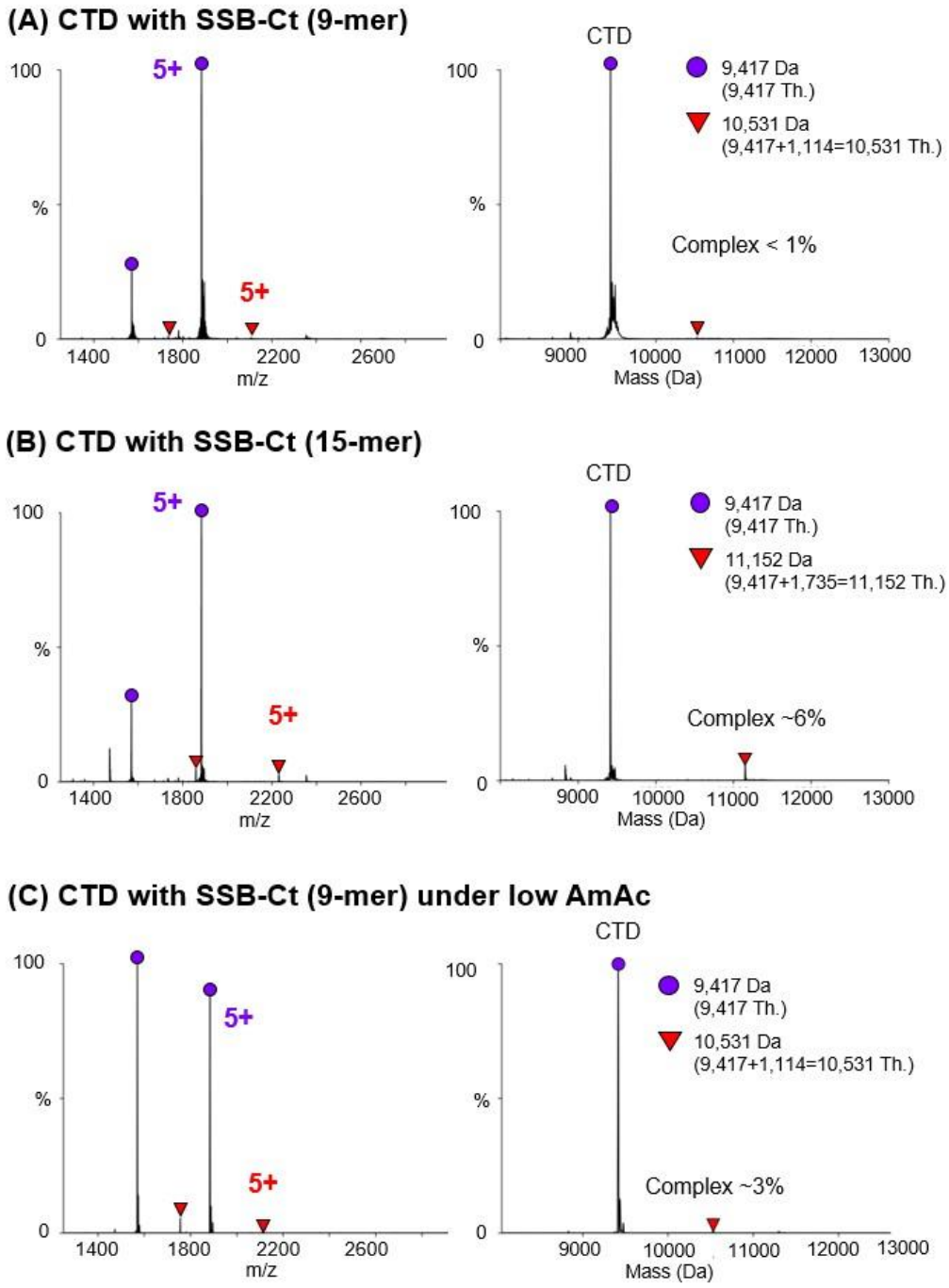

Figure 6. nMS of Redβ CTD in complex with SSB-Ct peptide. (A) The CTD–SSB-Ct complex was prepared by mixing 1.06 mM CTD with 1.7 mM CTD 9-mer peptide, and then diluted to 11/17 μM in 800 mM ammonium acetate. (**B**) The CTD–SSB-Ct complex was prepared as in panel A except with 15-mer peptide and at double the final concentration (20 μM CTD and 32 μM peptide). (**C**) The complex was prepared with 1.5 μM CTD and a 10-fold excess of 9-mer peptide (15 μM) in 200 mM ammonium acetate. All samples were analyzed by nMS with the following settings: R50k for A and B, R3k for C, IST5, TG1, low ion transmission. The experiments shown are representative of multiple experiments under different conditions, which all lead to similar conclusions.

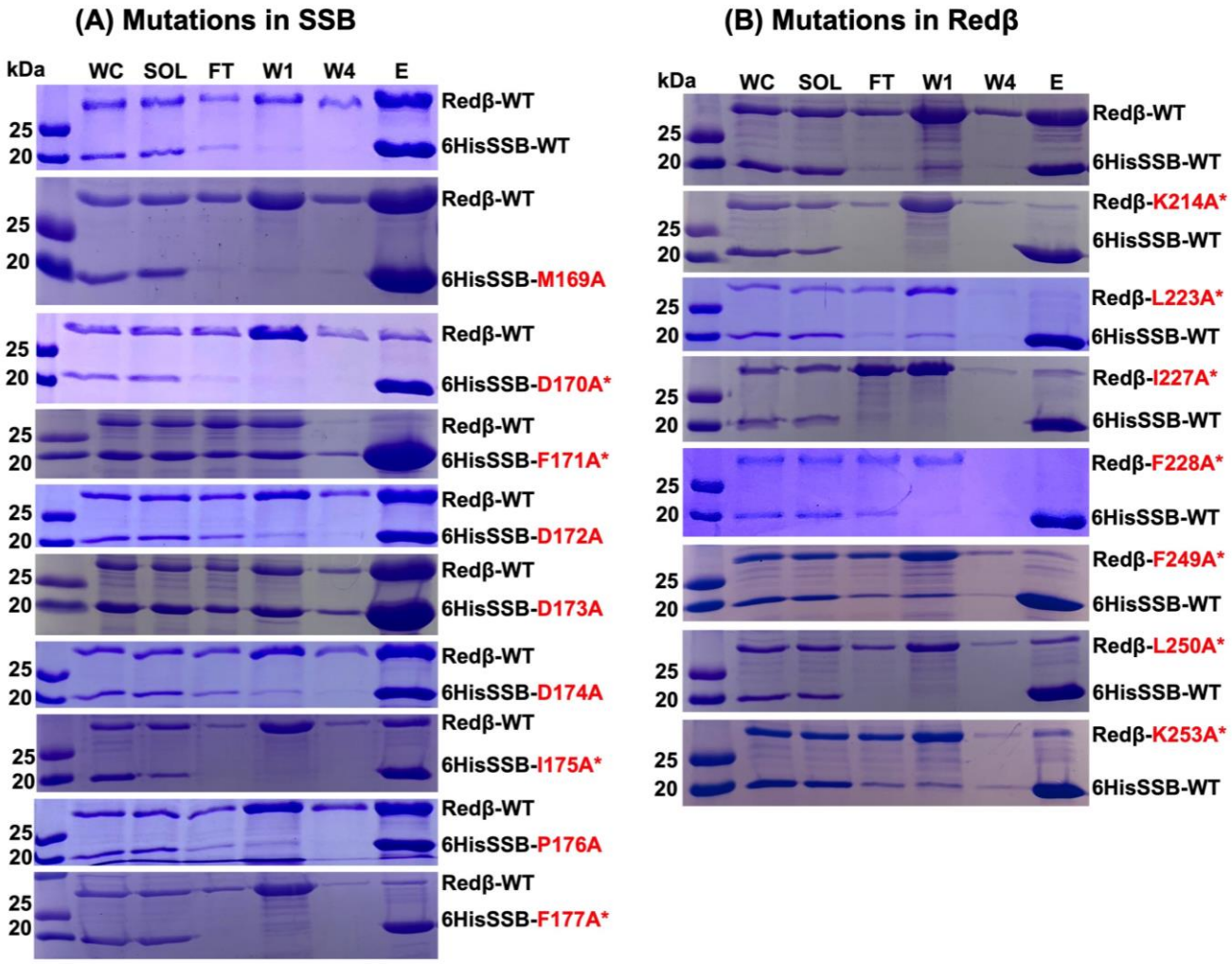

Figure 7. **Mutational analysis of the Redβ–SSB interaction by Ni-spin pull-down**. Separate batches of *E. coli* cells expressing untagged Redβ and 6His-tagged-SSB were mixed and lysed by sonication. The soluble portions of the lysates were loaded onto Qiagen Ni-NTA spin columns, washed four times with 30 mM imidazole (lanes labeled W1, W4 for the first and fourth washes), and eluted with 500 mM imidazole (lanes labeled E). An interaction between the two proteins is seen by co-elution of un-tagged Redβ with 6His-tagged-SSB in lane E. Protein variants of Redβ and SSB are indicated in red to highlight them, and variants deemed to have significantly disrupted the complex are indicated by an asterisk. None of the mutations had noticeable effects on soluble expression of the proteins, as essentially equivalent bands are seen for each protein when the whole cell ("WC") and soluble ("SOL") portions of each cell lysate were loaded. The experiments for each protein variant were performed at least twice with similar results.

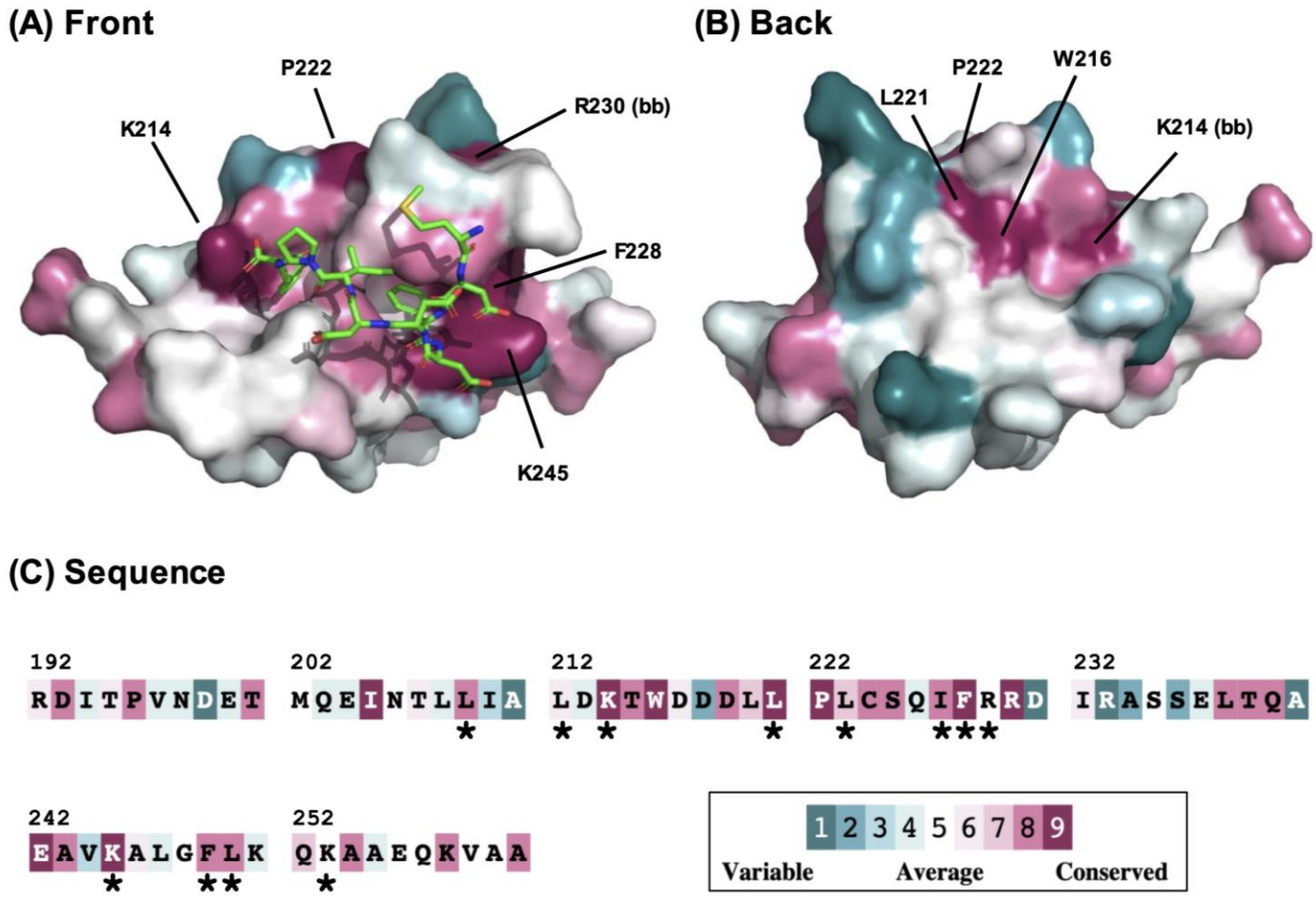

Figure 8. **Conservation analysis of the CTD**. (**A,B**) Front and back views of a molecular surface representation of the CTD–SSB-Ct complex color coded according to sequence conservation as determined by CONSURF (24). The invariant residues on the surface in dark purple are labeled. Cases where the backbone of the residues is exposed on the surface view are indicated by “bb” after the residue number. (**C**) The CTD amino acid sequence colored as for the structures in panels A and B. The variability scale was determined from a multiple sequence alignment of 60 homologous sequences meeting the min/max similarity hit criteria from the default parameters in CONSURF. Notice that the residues of the groove on the CTD underneath the SSB-Ct peptide are in general highly conserved, indicating that homologous RecT/Redβ family proteins likely use a similar groove for interactions with their host SSB and nuclease partner proteins.